Published in final edited form as:

Arterioscler Thromb Vasc Biol. 2023 June ; 43(6): 943–957. doi:10.1161/ATVBAHA.122.319025.

Autoimmune valvular carditis requires endothelial cell TNFR1 expression

Jessica L. Faragher[1,2,3], **Jennifer L Auger**[1,2,3], **Victoria Osinski**[1,2,3], **Lee A Meier**[1,2,3,4], **Brianna J Engelson**[1,3], **Maria M. Firulyova**[5,6], **Mayra I Gonzalez-Torres**[3,7], **Frank Brombacher**[8], **Konstantin Zaitsev**[6], **Aubyn Marath, MBBS, MS**[9], **Bryce A Binstadt**[*,1,2,3]

[1]Center for Immunology, University of Minnesota, Minneapolis, MN

[2]Department of Pediatrics, University of Minnesota, Minneapolis, MN

[3]University of Minnesota, Minneapolis, MN

[4]Department of Surgery, University of Colorado, Aurora, CO

[5]Almazov National Medical Research Centre, Saint-Petersburg, Russia

[6]Computer Technologies Laboratory, ITMO University, Saint Petersburg, Russia

[7]HCA Florida Kendall Hospital, Miami, FL

[8]International Centre for Genetic Engineering and Biotechnology, Cape Town, South Africa

[9]CardioStart International, Tampa, FL

Abstract

Background: Inflammation is a key driver of cardiovascular pathology, and many systemic autoimmune/rheumatic diseases are accompanied by increased cardiac risk. In the K/B.g7 mouse model of coexisting systemic autoantibody-mediated arthritis and valvular carditis, valve inflammation depends on macrophage production of TNF and IL-6. Here we sought to determine if other canonical inflammatory pathways participate and to determine whether TNF signaling through TNFR1 on endothelial cells is required for valvular carditis.

Methods: We first asked if type 1, 2, or 3 inflammatory cytokine systems (typified by IFNγ, IL-4, and IL-17, respectively) were critical for valvular carditis in K/B.g7 mice, using a combination of *in vivo* monoclonal antibody blockade and targeted genetic ablation studies. To define the key cellular targets of TNF, we conditionally deleted its main pro-inflammatory receptor, TNFR1, in endothelial cells. We analyzed how the absence of endothelial cell TNFR1 affected valve inflammation, lymphangiogenesis, and the expression of pro-inflammatory genes and molecules.

Results: We found that typical type 1, 2, and 3 inflammatory cytokine systems were not required for valvular carditis, apart from a known initial requirement of IL-4 for autoantibody production. Despite expression of TNFR1 on a wide variety of cell types in the cardiac valve, deleting

[*]Corresponding author binstadt@umn.edu, Office Phone: (612) 625-2953.

Disclosures

The authors have no disclosures or conflict of interest to declare.

TNFR1 specifically on endothelial cells protected K/B.g7 mice from valvular carditis. This protection was accompanied by reduced expression of vascular cell adhesion molecule (VCAM1), fewer valve-infiltrating macrophages, reduced pathogenic lymphangiogenesis, and diminished pro-inflammatory gene expression.

Conclusions: TNF and IL-6 are the main cytokines driving valvular carditis in K/B.g7 mice. The interaction of TNF with TNFR1 specifically on endothelial cells promotes cardiovascular pathology in the setting of systemic autoimmune/rheumatic disease, suggesting that therapeutic targeting of the TNF:TNFR1 interaction could be beneficial in this clinical context.

Graphical Abstract

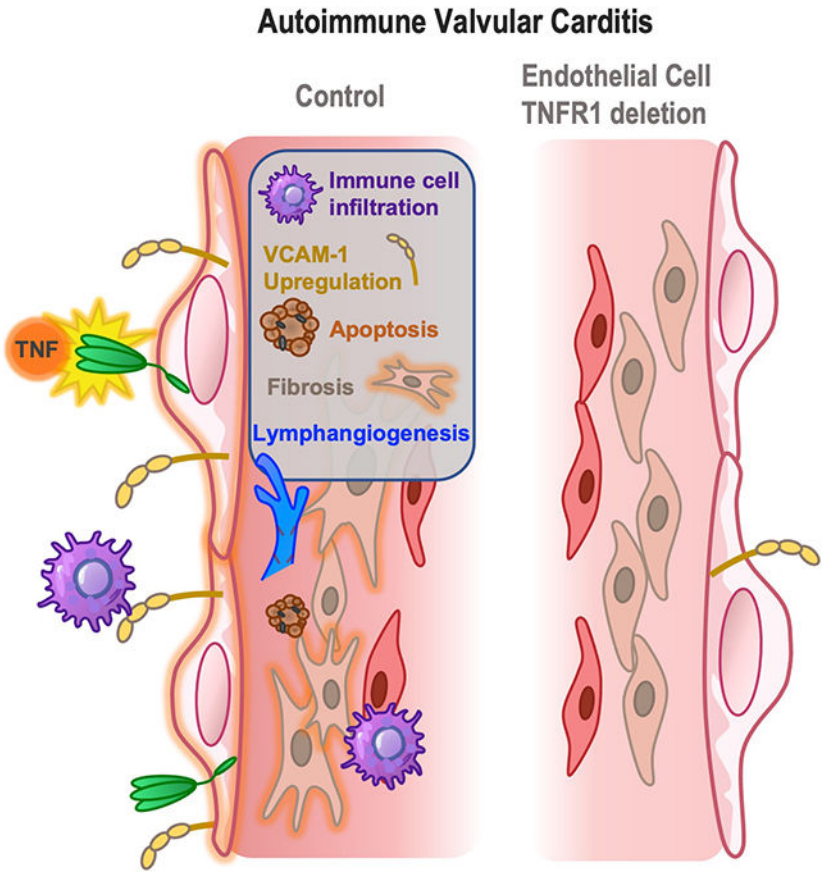

Keywords

Valvular carditis; TNF; Endothelial cell; Macrophage; Autoimmune

INTRODUCTION

Inflammation is a key contributor to many cardiovascular diseases [1-4]. Cardiac valve involvement is well known to occur in systemic autoantibody-mediated diseases such as systemic lupus erythematosus, antiphospholipid syndrome, and rheumatic heart disease (RHD) [5]. Autoimmune valvular carditis is characterized by inflammation and fibrotic remodeling of left sided heart valves, primarily the mitral valve [6]. This can culminate

in valvular insufficiency and/or regurgitation and increases susceptibility to bacterial endocarditis [7, 8]. RHD results from untreated group A *Streptococcus* infection and disproportionately affects low-income countries; it is a major cause of cardiovascular death in young patients with limited access to health services [9, 10]. More broadly, inflammatory cardiovascular pathology including atherosclerosis is the main source of morbidity and mortality among patients with rheumatic diseases [11].

The immunological mechanisms that mediate cardiovascular inflammation in these settings remain incompletely defined. Our group uses the K/B.g7 mouse model of spontaneous, co-existing autoantibody-driven arthritis and valvular carditis to dissect these mechanisms. This model consists of a transgene-encoded T-cell receptor that recognizes peptides from the ubiquitously expressed enzyme glucose-6-phosphate isomerase (GPI) presented by the MHC class II molecule I-A^{g7}. Subsequently, activated B-cells produce pathogenic anti-GPI autoantibodies [12]. The resulting autoantibody-induced joint and valve inflammation are mediated by distinct immunological effector pathways, allowing us to parse out valve-specific immune mediators [13].

We have previously shown that Fc receptor-mediated macrophage activation and subsequent IL-6 and TNF production are required for valvular carditis in this model [14, 15]. We have further shown that expression of TNFR1 on radioresistant stromal cells is critical for the development of valvular carditis, whereas blockade of TNFR2 actually exacerbated disease severity [15]. Here we explored many other cytokines and macrophage effector molecules and conclude that IL-6 and TNF are the predominant players; canonical type 1, 2, and 3 cytokine systems appear dispensable. Due to the pleiotropic and potent nature of TNF [16], we sought to determine its key cellular targets. Since TNF is well known to elicit endothelial activation [16, 17], we focused on TNFR1-expressing endothelial cells (ECs). Using an EC-specific (*Cdh5)* inducible Cre to conditionally delete TNFR1, we show that the interaction of TNF with TNFR1 on ECs is required for valvular carditis in K/B.g7 mice.

MATERIALS AND METHODS

Data Availability

The authors will make data and study materials supporting these findings available upon reasonable request. Please see the Major Resources Table in the Supplement.

Animals

Animal studies were approved by the University of Minnesota Institutional Animal Care and Use Committee (IACUC protocols 1805-35885A, 1506-32700A and 1207A17481). Standard specific pathogen free (SPF) housing was used. Male and female mice were used in approximately equal numbers. KRN T cell receptor (TCR) transgenic (‘KRN’) and C57BL/6:I-Ag7 MHC class II congenic (‘B.g7’) were gifts from D. Mathis, C. Benoist, and the Institut de Génétique et Biologie Moléculaire et Cellulaire (IGBMC), Illkirch-Graffenstaden, France. *Il4ra*$^{fl/fl}$ (‘*Il4ra-floxed’*, mice with floxed *Il4ra* alleles, subsequently backcrossed onto the C57Bl/6 genetic background) [18] have been previously described. *Il17a/f*$^{-/-}$ (mice with genetic deletion of both *Il17a* and *Il17f*) were a gift from Immo Prinz

and have been previously described [19]. *Il17ra*$^{-/-}$ (mice with deletion of the gene encoding IL17RA) were a gift from Amgen. The following lines were purchased from The Jackson Laboratory: B6J.B6N(Cg)-*Cx3cr1*$^{tm1.1(cre)Jung}$/J ('*Cx3cr1-Cre'*, stock # 025524), C57BL/6-Irf5^{tm1Ppr}/J ('*Irf5*$^{fl/fl}$', '*Irf5*-floxed', stock # 017311), B6.129S7-Ifng^{tm1Ts}/J ('*Ifng*$^{-/-}$', stock # 002287), B6(Cg)-Tlr4$^{tm1.2Karp}$/J ('*Tlr4*$^{-/-}$',stock # 029015), B6.129P2-Nos2^{tm1Lau}/J ('*Nos2*$^{-/-}$', stock #002609), C57Bl/6-Il4^{tm1Nnt}/J ('*Il4*$^{-/-}$', stock # 002518), C57Bl/6 (stock # 000664), and ROSA$^{mT/mG}$ (stock # 007676).

The TNFR1 floxed mice (*Tnfrsf1a*$^{tm3.1Gkl}$) were generated by George Kollias and obtained from EMMA/INFRAFRONTIER (stock 07099) [20]. The VE Cadherin-Cre line for tamoxifen-inducible Cre-recombinase expression under regulation of the vascular endothelial cadherin promoter (*Cdh5-Cre*ERT2^{Ykub}) has been previously described [21] and was a gift from Dr. Yoshiaki Kubota. Endothelial cell lineage-tracing was performed using K/B.g7 *Cdh5*-Cre/ER^{T2} ROSA$^{mT/mG}$ mice with either fully floxed (TNFR1$^{fl/fl}$) or control (TNFR1$^{wt/fl}$) mice.

Tamoxifen administration

Cre-recombinase expression was induced via intraperitoneal injection of 200 μg tamoxifen (T5648, Sigma-Aldrich) dissolved in corn oil (C8267, Sigma-Aldrich) vehicle. Animals were treated once daily for three days starting at 3 or 6 weeks of age, and harvested 5 weeks later. Tamoxifen was dissolved overnight in 37°C incubator and kept in 4°C between injections. Suspension was warmed in 37°C incubator prior to injection.

Monoclonal antibody (mAb) blockade studies

The monoclonal anti-IL-4 antibody (clone 11B11) for *in vivo* use was purchased from BioXcell. Anti-IL-13 (Tanox IL-13 (Mo):9517) was a gift from Genentech, Inc (South San Francisco, CA, USA). Isotype control antibodies were purchased from Jackson Immunoresearch, Inc. Antibodies were diluted to 1 mg/ml in phosphate-buffered saline (PBS) and 0.2 ml (200 μg) was injected intraperitoneally twice weekly.

Mouse heart collection, sectioning, and histology

Immediately following euthanasia, the chest cavity was opened, descending aorta was severed to allow blood to exit, and hearts were perfused with 10 mL cold PBS. Hearts were removed, embedded in OCT medium, and frozen in a slurry of dry ice and 2-methyl-butane. Lineage-traced *Cdh5*-Cre/ER^{T2} ROSA$^{mT/mG}$ hearts were fixed in 4% paraformaldehyde (PFA) for one hour immediately after removal. Hearts were washed in PBS and then incubated in a 15% sucrose solution overnight at 4°C and then transferred to a 30% sucrose solution for 4 hours at 4°C. Hearts were washed in PBS before embedding in OCT and frozen over a dry ice slurry.

Frozen murine hearts were cryosectioned in the coronal plane to 7 or 8 μm thick slices (Leica CM3050 S) and transferred to glass slides (12-550-15, Thermo Fisher Scientific). Sections were stored at −80°C until use.

Frozen sections were allowed to air dry and were fixed in cold acetone prior to hematoxylin and eosin (H&E) staining (Vector, H-3404) according to manufacturer's protocol. Mitral valve thickness was measured using H&E stained sections as described previously [22]. Trichrome staining (abcam, ab150686) was performed following 4% PFA fixation according to manufacturer's protocol. Histologic sections were cleared in xylene and mounted with VectaMount permanent mounting media (Vector, H-5000). CellSens imaging software (Olympus) and an Olympus BX51 microscope were used for brightfield image acquisition.

Immunofluorescent staining of mouse tissue

Sections of mouse cardiac tissue were prepared for immunofluorescent (IF) staining as described previously [13]. Fresh frozen mouse cardiac sections were fixed with cold 4% PFA for 10 minutes then washed in three changes of PBS. Non-specific binding was blocked with 5 μg/ml anti-CD16/32 (rat monoclonal [2.4G2], Tonbo Biosciences) diluted in a rinse buffer of 2% BSA, 5% normal donkey serum (NDS), and 0.1% Tween-20. For biotinylated antibodies, this blocking step was followed by biotin blocking (E21390, Invitrogen) per manufacturer's protocol. Antibodies were diluted in rinse buffer described above and incubated overnight at 4°C. The following day sections were washed in PBS and secondary antibody diluted in rinse buffer and incubated at room temperature for 45 minutes. Nuclei were stained with 1 μg/mL Hoechst (33342, Thermo Fisher Scientific). Slides were washed in PBS and mounted with VECTASHIELD Plus Antifade mounting medium (H-1900). Images were acquired within 24 hours of mounting on a Leica DM6000B epi-fluorescence microscope with LAS X (Leica) software. A 20x objective lens was used to acquire between 10-18 focal planes (z-axis) with tile-scan mode employed to image the entirety of each valve. Exposure times were matched to species-matched isotype control samples. Primary and secondary antibodies used are listed in the Online Supplement. Representative images displayed in figures were selected based on the continuous tissue morphology and the valve thickness measurements being near the average thickness of the group.

Immunofluorescent staining of human tissue

De-identified human cardiac valve samples were acquired by CardioStart International during charitable missions in countries with high incidences of RHD. Additional de-identified non-rheumatic control valve samples obtained from patients undergoing surgical correction for non-inflammatory valve conditions. The samples were collected following the patient consent procedures approved by University of Minnesota IRB protocol 1307M39481. Human mitral valve tissue was processed as described previously[15]. Valve samples were formalin fixed and paraffin embedded prior to sectioning. Slides were deparaffinized in 2 changes of xylene for 10 minutes each, or until paraffin had dissolved completely. Sections were rehydrated for 5 minutes each in 100%, 95%, 70%, 50% ethanol: dH_2O gradient and rinsed twice in dH_2O. Antigen retrieval was performed in citrate buffer (10mM Citric acid anhydrous, 0.05% Tween-20, pH 6.0) for 30 minutes at 95°C. Sections were allowed to cool in buffer at room temperature for 30 minutes, washed in PBS, permeabilized in 0.1% Tween-20 for 10 minutes, and washed again. Endogenous Fc receptor expression was blocked (Innovex Biosciences, NB309) for 40 minutes at room temperature. Primary antibody was diluted in the same rinse buffer described above and incubated on sections overnight at 4°C. The next day, slides were washed in PBS prior to

adding secondary antibody diluted in rinse buffer for 1 hour at room temperature. Secondary antibody was washed off with PBS before nuclear counterstain with Hoechst. Slides were washed again in PBS before being coverslipped with Vectashield plus. Coverslipped sections were chilled for 30 minutes in 4°C prior to imaging. Exposure times were matched to species-matched isotype control samples. Representative images of human valve tissue were selected based on the sample's proximity to the average measurement.

In situ zymography

Fresh frozen mouse cardiac tissue was used to assess active MMP2/9 activity. DQ gelatin with fluorescein conjugate (D12054, Invitrogen) was diluted to a working concentration of 2 ug/mL in MMP activity buffer (100 mM NaCl, 10 mM CaCl2, 20 μM ZnCl, 0.05% Tween-20 and 100 mM Tris-HCl at pH 7.5). Control slides were incubated with substrate dilution containing 20 mM EDTA to inhibit MMP activity. Following two 5-minute PBS washes, an equal amount of diluted substrate was added to each section. Slides were incubated in a dark humidity chamber at 37°C for 1 hour. Following incubation, substrate was rinsed off of slides with dH_2O. Slides were washed in two changes of PBS for 5 minutes each and fixed in 10% formalin for 5 minutes. Following fixation, slides were washed in dH_2O and PBS as previously described. Slides were mounted with VECTASHIELD containing DAPI (H-2000) for nuclei staining. Slides were viewed on Leica DM6000B epi-fluorescence microscope and 20x images were taken for analysis.

Image analysis

The Fiji distribution of ImageJ (NIH) was used for image analysis. The image analyses are based on methods described previously [15]. Species-matched isotype control samples were analyzed in parallel. Greyscale maximum-intensity z-projections were generated for each channel of interest. Linear adjustments of brightness were applied equally to all images and isotype control images. Using the maximum-intensity projection in 8-bit image format, the mitral valve leaflet region of interest (ROI) was outlined manually for subsequent analysis.

Expression of VCAM-1 staining as a percent of MV area was quantified as described previously [23]. Briefly, images were converted to a binary format and then positive area within the MV ROI was calculated in FIJI.

The numbers of CD64+ cells and total cells were quantified using FIJI. Within FIJI, images were subjected to minimal background subtraction with rolling ball (radius of 15 pixels for CD64 and 10 for DAPI channels) to reduce background signal. The threshold function was applied to convert images to a binary, with the same parameters applied to all images of the same channel. CD64 binary images were additionally reduced of non-specific signal applying FIJI's "despeckle" processing. The binary watershed mask was applied to the DAPI channel to ensure proper division of individual cells. The analyze particles function in FIJI was applied with the pixel^2 size set at 20-infinity for CD64 and 0-infinity for DAPI. These parameters differ slightly due to the more irregular morphology of CD64 staining. Cell counts for each ROI within the image were recorded. This method was employed for all immunofluorescent imaging data depicting cell counts.

Caspase-3 cell counts were performed on images merging cleaved caspase-3 and nuclei channels. Lymphatic vessel formation was assessed with merged LYVE-1, VEGFR3, and nuclear staining channels. Vessels were counted as a minimum of three consecutive cells co-expressing LYVE-1 and VEGFR-3.

Signal intensity of images was measured in FIJI using 8-bit grayscale images. Following selection of the mitral valve ROI, the “measurements” feature was used to collect the mean gray value of the pixels within the ROI.

Cardiac tissue digestion

After euthanasia, hearts were perfused with 5 mL cold PBS, excised, and placed in 0.5 mL cold RPMI medium containing GlutaMAX supplement (Thermo Fisher Scientific) with added 3% fetal bovine serum (FBS, Thermo Fisher Scientific), and 10 mM HEPES (Thermo Fisher Scientific). The mitral valve was isolated as previously described [15]. Tissue of interest was placed in 1 mL of RPMI/ FBS/ HEPES buffer with 500 U/ml collagenase-2 (Worthington Biochemical) and 20 U/ml DNase I (Worthington Biochemical), pre-warmed to 37°C for digestion. Heart was quickly minced in solution with scissors before being incubated in dry bath at 37°C for 1-hour with intermittent trituration using a P-1000 pipette to digest tissue. Samples were centrifuged for 5 minutes at 300xg at 4°C. Pellets were washed once with 2% BSA. Erythrocytes remaining in the pellet were lysed using 0.3 ml ammonium chloride-potassium (ACK) lysis buffer (150 mM NH_4Cl, 10 mM $KHCO_3$, 0.10 mM EDTA) at room temperature for 3 minutes and quenched with 1 mL 2% BSA. The samples were centrifuged at 300xg for 5 minutes at 4°C. Cells were resuspended in 1 mL 2% BSA and filtered through 70-micron filters. Samples were centrifuged and filtered through 40- micron filters and counted. Cells were resuspended in 90 μL of 0.5% BSA and 10 μL of CD45 MicroBeads (130-052-301, Miltenyi Biotech) were added and processed according to manufacturer’s protocol. Magnetically labeled cells were added to an LS Column (130-042-401, Mitenyi Biotech) on a MidiMACS™ Separator to deplete CD45-positive cells. $CD45^+$ cells were flushed from column for further downstream processing. Remaining cells were then incubated with CD31 MicroBeads (130-097-418, Miltenyi Biotech) according to manufacturer’s protocol. Cells were added to LS column to enrich $CD31^+$ endothelial cells. 200,000 cells from a pool before any sorting and a pool following $CD45^+$ depletion and $CD31^+$ enrichment were taken for flow cytometric analysis. The remaining samples proceeded to RNA isolation and cDNA generation.

Flow cytometric analysis of sorted cells

Sorted samples were added to a 96-well plate and were washed with 0.5% BSA and centrifuged at 300xg for five minutes at 4°C. Samples were resuspended in 5 μg/mL anti-CD16/32 (rat monoclonal [2.4G2], Tonbo Biosciences) in a total of 200 μL 0.5% BSA for 15 minutes on ice. Following block, antibodies were added and incubated on ice protected from light for 30 minutes (antibodies used are listed in Online Supplement). Samples were centrifuged and resuspended in a 1:1000 dilution of viability dye for 15 minutes on ice. Samples were washed and fixed (Cytofix/Cytoperm, BD Biosciences) before a final wash and resuspension in 2% BSA. A Fortessa X-30 H0081 (BD Biosciences) cytometer with FACSDiva software was used for data acquisition. Compensation was configured using

single-stain compensation beads (UltraComp eBeads Compensation Beads, Thermo Fisher Scientific). Flow cytometric data were analyzed using FlowJo software (v 10.8.1).

RNA isolation and cDNA generation

Following the preparation of a single cell suspension, cells were pelleted and resuspended in 1 mL of TRIzol (Invitrogen, catalog #15596026) and RNA isolation was performed according to manufacturer's protocol (MAN0001271). RNA $A_{260/280}$ ratio was assessed with a NanoDrop OneC (Thermo Scientific). cDNA synthesis was then performed using the SuperScript™ IV First-Strand synthesis system (Thermo Fisher, 18091050) following manufacturer's protocol (MAN0013442). cDNA samples were stored at −20°C until use.

RT-qPCR

Real time, quantitative PCR (qPCR) was used to quantify gene expression. 3 μM of forward and reverse primers (sequences in Major Resources Table in Supplement) were combined with cDNA from each sample and FastStart Universal SYBR Green with ROX (Roche) according to manufacturer's protocol (version 06) in 384-well plates (Bio-Rad HSP3805). PCR reactions were run using a Bio-Rad CFX384 with an annealing temperature of 60°C for all primer sets. Samples were run in duplicate, and values were averaged for analysis. Data were calculated by the ΔΔCt method and expressed in arbitrary units normalized to β-actin levels.

scRNA sequencing analysis

Following valve isolation and tissue processing to a single cell suspension as described above, live, single cells were sorted and prepared using a Single Cell 3' Reagent Kit following the manufacturer's protocol (10x Genomics). Sequencing was conducted with the NovaSeq 6000 Sequencing System (Illumina) and a MiSeq instrument was used to assess sequencing quality. All sequencing and post-sequencing data clean-up and processing was conducted by the University of Minnesota Genomics Center (UMGC).

Alignment, barcode assignment, and UMI counting with Cell Ranger (version 3.1.0) [24] were used for count matrix generation. For alignment, a *Mus musculus* genome mm10-3.0.0 was used as a reference. Barcodes in all samples that were considered to represent noise and low-quality cells were filtered out using the default knee-inflection approach available in default Cell Ranger analysis.

For downstream analysis, Seurat package (version 3.1.0) [25-28] was used. Genes expressed in less than 3 cells were filtered from the expression matrices along with cells that expressed less than 200 genes. Finally, cells with a mitochondrial percentage more than highest confidence interval for scaled mitochondrial fraction were filtered out.

Each sample was normalized using the SCTransform function with mitochondrial fraction as a variable to regress out in a second non-regularized linear regression. For integration purposes, highly variable genes across the samples were identified using the SelectIntegrationFeatures function with the number of features equal to 2000. Then the object was prepared for integration (PrepSCTIntegration function), the anchors were found

(FindIntegrationAnchors function) and the samples were merged into the whole object (IntegrateData function).

Dimensionality was reduced by principal component analysis (PCA), and the first 20 principal components were used further to generate uniform manifold approximation and projection (UMAP) dimensionality reduction. The clustering procedure was performed by FindNeighbors and FindClusters (resolution 0.6). Some of the output clusters were manually merged based on the marker genes' expression (e.g., *Tcf21*+ clusters were labeled as the *Tcf21*+ fibroblasts) after biological annotation of each cluster (e.g., *Cdh5*+ clusters were annotated as VECs, the *Cd3d*+ cluster as T cells, proliferating cells were identified based on the expression of Mki67, etc.).

Sequencing data has been uploaded to the National Center for Biotechnology Information (NCBI) Gene Expression Omnibus (GEO) for public access under accession code GSE221197.

Arthritis assessment

Clinical arthritis scoring and mouse ankle thickness assessments were performed weekly beginning at three weeks of age. Arthritis scoring was conducted using a 12-point system as previously described [22]. Ankle thickness was measured using a dial gauge (Käfer, model J15) following a previously described method [33].

Evaluation of anti-glucose-6-phosphate isomerase antibody titers and serum TGF- β1 levels

Following euthanasia, blood was collected and centrifuged at 300xg for 5 minutes for plasma collection. Anti-GPI antibody titers were quantified using an enzyme-linked immunosorbent assay (ELISA) as described previously[34, 35]. A 96-well plate was coated overnight at 4°C with 5 ug/mL of GPI diluted in PBS. The following day, plate was blocked for 1 hour at room temperature with 2% BSA. Serum samples were diluted to 1:100 in PBS and incubated for 1 hour at room temperatures. Following incubation, plate was washed three times with 0.5% BSA and washed once in PBS. Secondary antibody, alkaline phosphatase anti-mouse IgG, was diluted 1:2500 in PBS and incubated for 1 hour at room temperature. Following incubation, plate was washed as previously described. A phosphatase substrate tablet was dissolved in AP buffer and added to the plate to develop color. Plate was read on a microplate reader (BioRad iMark) at 415nm . Samples were plated in duplicate and averaged for analysis. The average of the "blank" wells were subtracted from each sample. Absorption values were normalized by setting the average of the control group to one. Mouse sera were assayed for circulating levels of TGF-β1 via a solid phase sandwich ELISA (DY1679, R&D Systems) following manufacturer's instructions. Assay was read at 450 nm on a microplate reader.

Statistics

Statistical analyses were done on GraphPad (Prism v. 9.4.0). Because of small sample sizes, normality was not presumed and therefore nonparametric tests were used. For comparing two groups at a single time point, Mann-Whitney tests were used. For three

groups, a Kruskal-Wallis test followed by Dunn's multiple comparisons test was used. For longitudinal arthritis data, two-way repeated measures ANOVA with Geisser-Greenhouse correction was performed, followed by a Šídák multiple comparisons test. Statistical significance was defined as $p<0.05$. Exact P values are reported in figures, rounded to two significant digits.

RESULTS

Typical Type 1, 2, 3 inflammatory signals are dispensable for arthritis and cardiac valve disease in K/B.g7 mice.

TNF and IL-6 are critical drivers of autoimmune valvular carditis in the K/B.g7 mouse model. We have shown previously that binding of immune complexes to activating Fc receptors stimulates a Syk-dependent signaling pathway leading to macrophage TNF and IL-6 production, and that antibody blockade of IL-6 or TNF blocks valve inflammation and fibrosis [14, 15]. We first sought to define the potential contribution of other cytokines and related pro-inflammatory molecules in this model, using the general framework of type 1 (IFNγ), type 2 (IL-4, IL-13), and type 3 (IL-17) inflammatory pathways.

We first generated K/B.g7 mice with genetic deletion of key type 1 inflammatory mediators, including interferon gamma (*Ifng*), toll-like receptor-4 (*Tlr4*), or inducible nitric oxide synthase (iNOS, encoded by *Nos2*). The severity of valvular carditis in each of these lines was not statistically significantly different from heterozygous littermate controls (Figure 1A-1C). Arthritis development and anti-GPI autoantibody production were also not statistically significantly different (Online Figures S1A-F).

Irf5 is a master regulator of a transcriptional program leading to 'M1-like' macrophage polarization, associated with type 1 inflammatory responses [36]. We have previously demonstrated a critical role for CX3CR1-expressing macrophages in valvular carditis [15]. We found that K/B.g7 mice with conditional deletion of *Irf5* in MNPs (*Cx3cr1-Cre*$^{+}$:*Irf5*$^{fl/fl}$) developed valve inflammation, arthritis, and anti-GPI autoantibodies that was not statistically significantly different compared to littermate control mice lacking *Cre* expression (*Cx3cr1-Cre*$^{-}$:*Irf5*$^{fl/fl}$) (Figure 1D and Online Figures S1G and S1H). Collectively, these results demonstrate that typical type 1 inflammation is dispensable for valvular carditis and arthritis in K/B.g7 mice.

With respect to type 3 inflammation, we have previously shown that the initiation and progression of arthritis and anti-GPI autoantibody production do not require IL-17A/F or T_H17 cells [37]. We similarly found that K/B.g7 mice with constitutive deletion of the genes encoding both IL-17A and IL-17F or the gene encoding their receptor, IL-17RA, developed mitral valve inflammation not statistically significantly different from control mice (Figure 1E and 1F). Thus, type 3 inflammatory signals are also dispensable for systemic inflammatory disease in K/B.g7 mice, including valvular carditis.

We next asked whether type 2 inflammatory signals are required. Previous work has shown that IL-4 is required for autoantibody production and arthritis development in this model [38]; we confirmed that finding. Not surprisingly, IL-4 deficient K/B.g7 mice also did not

develop valvular carditis, consistent with the dependence of valve disease on autoantibody formation (data not shown). We therefore sought to interrogate the type 2 cytokine system in K/B.g7 mice with intact autoantibody production. Using K/B.g7 mice in which spontaneous autoantibody production had already begun, we administered blocking antibodies to IL-13 or IL-4; these treatments had no statistically significant effect on valve inflammation (Figure 2A and 2B) nor arthritis severity scores (Online Figure S2). Similarly, the severity of valvular carditis and arthritis was not statistically significantly different from controls in mice with macrophage-specific deletion of either IL-4Rα, a receptor subunit shared by the receptors for IL-4 and IL13, or of Arginase-1, a key driver of type 2 (M2) macrophage polarization [39] (Figure 2C and 2D and Online Figures S2 and S3). Thus, we conclude that type 2 cytokine signaling, despite being required for initial autoantibody production in this model, is dispensable for the later development of arthritis and valvular carditis in mice with intact autoantibody production.

These findings demonstrate that canonical type 1, 2, and 3 cytokine signaling pathways are not required for valvular carditis in K/B.g7 mice. Based on these findings and our prior studies, we conclude that the binding of immune complexes to activating FcRs is a main macrophage activation pathway in this model, and that TNF and IL-6 are the dominant pro-inflammatory cytokines at play.

TNFR1 on endothelial cells is critical for valvular carditis

We therefore sought to identify the key cell type(s) responding to TNF to drive valvular carditis. We showed previously that expression of TNFR1 on radioresistant cells was necessary for mitral valve inflammation, whereas expression of TNFR1 on bone marrow-derived cells was not [15]. Single cell RNASeq analysis of isolated mitral valves revealed a heterogeneous cellular makeup (Figure 3A), as expected. Figure 3B demonstrates the expression of *Cdh5*, the gene encoding the endothelial cell Cre driver we used to conditionally delete TNFR1. Expression of *Tnfrsf1a*, the gene encoding the p55 subunit of TNFR1, was observed on numerous cell types including endothelial cells, fibroblasts, and immune cells (Figure 3C). In contrast, expression of TNFR2 (encoded by *Tnfrsf1b*) was much more restricted (Figure 3C). Expression of the gene encoding TNF itself was limited primarily to myeloid cells, identified by expression of CD45 (encoded by *Ptprc*) and *Fcgr1* which encodes CD64 (Figure 3D, E). In contrast, expression of IL-6, the other key cytokine driving valvular carditis, was more widespread (Figure 3E).

We next examined TNFR1 expression in mitral valves from human patients with RHD as well as controls without inflammatory valve disease. We found expression of TNFR1 near the endothelial surface of the valves, as well as deeper in the interstitium (Online Figure S4A-D). As expected based on expression of TNFR1 on many cell types, the fraction of total cells that expressed TNFR1 did not differ between rheumatic and non-rheumatic samples (Online Figure S4E). However, the density of TNFR1+ cells, i.e. the number of TNFR1+ cells/valve area, was significantly greater in the rheumatic samples, consistent with the presence of an inflammatory infiltrate (Online Figure S4F).

Because endothelial cells are radioresistant, are a predominant cell type in non-inflamed cardiac valves, and are key contributors to other types of cardiovascular inflammation,

we asked whether endothelial cell expression of TNFR1 was required for valvular carditis to develop. We generated K/B.g7 mice allowing conditional ablation of TNFR1 in endothelial cells, using tamoxifen-inducible vascular endothelium cadherin (VE-Cad, *Cdh5*)-driven CreER^{T2} and floxed alleles of the gene encoding TNFR1 (*Tnfrsf1a*), here termed TNFR1$^{\Delta Cdh5}$. Littermate K/B.g7 mice expressing two floxed alleles encoding TNFR1 with no Cre construct were used as controls (TNFR1$^{fl/fl}$). The *Cdh5*-Cre construct targets all *Cdh5*-expressing endothelial cells in the mouse; using a fate-reporting mouse, we verified that *Cdh5*-Cre-mediated deletion occurs in endothelial cells situated on the valve surface (Online Figure S5). Using Magnetic Activated Cell Sorting (MACS) followed by qPCR, we verified that tamoxifen administration resulted in deletion of *Tnfrsf1a* in CD31+ endothelial cells but not in other cell types (Figure 4A). Prior to and following magnetic sorting, cells were evaluated via flow cytometry for purity of the endothelial cell population (Online Figure S6).

We administered tamoxifen to 3-week-old mice to determine if the absence of TNFR1 on endothelial cells could prevent the development of valvular carditis and to 6-week-old mice to determine if it would reduce the severity of established disease (Figure 4B). With each regimen, we found that the absence of TNFR1 on endothelial cells significantly reduced the degree of mitral valve thickening (Figure 4C and D, right), though not entirely to the thickness of mitral valves in littermate control non-arthritic mice lacking the KRN TCR transgene [13]. This was accompanied by reduced collagen deposition (Figure 4C and D, left), indicating reduced fibrosis. We verified that this protection from valvular carditis and fibrosis was not due to impaired anti-GPI autoantibody production (Figure 4E and 4F, right). Intriguingly, despite the well-known role of TNF in promoting arthritis in some mouse models, it is not a key driver of arthritis in the K/B.g7 model or its derivative, serum transferred arthritis [15, 40-42]. Consistent with this, the absence of TNFR1 on endothelial cells did not result in a statistically significant difference in the severity of arthritis in this model (Figure 4E and 4F, left). Thus, the TNF:TNFR1 interaction is required for the pathogenesis of valvular carditis but not arthritis in this model. Furthermore, despite expression of TNFR1 on many cell types in the cardiac valves (see Figure 3), its expression specifically on endothelial cells is critical for disease pathogenesis.

In the course of these studies, we also evaluated other endothelial cell receptors that might promote valvular carditis and/or fibrosis. Consistent with our other results, K/B.g7 mice lacking IL-4Rα on endothelial cells developed valvular carditis, arthritis, and anti-GPI autoantibodies that were not statistically significantly different from controls (Online Figures S7A-D). Additionally, we investigated TGFβR2, a driver of fibrosis in many systems; expression of TGFβR2 on endothelial cells was also not required for valvular carditis, nor did it significantly affect circulating levels of TGFβ (Online Figures S7E-I).

TNFR1 activates endothelial cells to promote valve inflammation and lymphangiogenesis

TNF stimulates vascular endothelial cells to upregulate expression of adhesion molecules, resulting in extravasation of immune cells into tissues. We have previously shown that the VLA-4:VCAM1 interaction is required for valvular carditis in this model [15]. In K/B.g7 mice lacking TNFR1 on endothelial cells, the expression of VCAM1 was reduced (Figure 5A and

Online Figures S8A and S10A). Additionally, infiltration of macrophages was significantly reduced (Figure 5B and Online Figures S8B, S9A, and S10B). These findings suggest that TNF binding to TNFR1 on endothelial cells upregulates expression of VCAM1 to promote influx of key inflammatory cells, primarily macrophages in this model. We have previously demonstrated that mitral valve inflammation is accompanied by accumulation of apoptotic cells [23]. Consistent with this, the number of cleaved caspase-3 apoptotic cells was significantly reduced in TNFR1$^{\Delta Cdh5}$ mice compared to controls (Figure 5C and Online Figures S8C and S10D).

Furthermore, we have recently discovered that valvular carditis is accompanied by the growth of new lymphatic vessels into the valve interstitium and that blockade of lymphatic formation reduces the severity of valve inflammation (Osinski et al, submitted). Given the established role of TNFR1 in regulating lymphatic growth and function [43], we asked if the absence of TNFR1 on endothelial cells impacted lymphangiogenesis in K/B.g7 mice. We found significantly reduced numbers of lymphatic vessels in K/B.g7 mice lacking TNFR1 on endothelial cells relative to control mice (Figure 5D and Online Figures S8D, S9B-C, and S10C). It is possible that TNF directly promotes lymphangiogenesis by binding to TNFR1 on endothelial cells or that lymphangiogenesis is stimulated indirectly by other factors present in the inflamed cardiac valve.

Endothelial TNFR1 induces inflammatory and vascular remodeling genes

We next analyzed how the absence of TNFR1 on endothelial cells affected expression of genes involved in matrix remodeling, inflammation, and vascular remodeling, since each of these processes occurs in the inflamed mitral valves.

Matrix metalloproteinases (MMPs) act to degrade extracellular matrix, but also act on matrix associated proteins like growth factors, cytokines, and chemokines. MMP activity is balanced by tissue inhibitors of matrix metalloproteinases (TIMPs). Despite reduced collagen deposition in the absence of endothelial TNFR1 expression (see Figure 4), expression of genes encoding MMPs and TIMPs was not statistically significantly different compared to controls (Figure 6A). Multiple testing correction was not used for statistical analysis. Using in situ zymography, we found that the activity of MMP2 and MMP9 in the valve was not significantly altered in the absence of endothelial cell TNFR1 expression (Online Figures S11A-D). Similarly, phosphorylation of SMAD2, which occurs downstream of TGFβ receptor signaling, was not statistically significantly different in mice lacking endothelial cell TNFR1 expression compared to controls (Online Figures S11E-H). These findings suggest that the reduction in fibrosis in this setting is not primarily due to effects on matrix remodeling pathways.

With respect to induction of inflammatory genes, we found reduced expression of IL-6 in mitral valves of TNFR1$^{\Delta Cdh5}$ mice relative to controls, consistent with TNF and IL-6 acting in series. Endothelial cell TNFR1 is a well-known activator of the pro-inflammatory transcription factor NF-κB, and mitral valves from TNFR1$^{\Delta Cdh5}$ mice had significantly reduced expression of *Nfkb1* and the gene encoding its active co-unit RelA (Figure 6B). NF-κB controls endothelial activation by inducing adhesion molecule expression. In concordance with our immunofluorescent staining (see Figure 5A and Online Figure S8A),

Vcam1 transcript levels were reduced in the mitral valves of TNFR1$^{\Delta Cdh5}$ mice relative to controls (Figure 6B).

TNF is known to induce vascular remodeling in a variety of disease contexts [44, 45], and we have observed increased angiogenesis and lymphatic growth in inflamed K/B.g7 mitral valves (Osinski et al, submitted). Vascular endothelial growth factor C (VEGF-C) signals through the receptors VEGFR-3 and neuropilin-2 to induce and maintain lymphatic vessels [46]. Angiopoietin-1 and its receptor (encoded by *Tie1*) also contribute to angio- and lymphangiogenic processes and more broadly act to maintain endothelial stability and permeability [47, 48]. Expression of the genes encoding each of these molecules was significantly reduced in TNFR1$^{\Delta Cdh5}$ mitral valves compared to controls (Figure 6C). We therefore conclude that the reduction in fibrosis seen in the absence of endothelial cell TNFR1 expression stems more from effects on inflammatory and vascular remodeling pathways rather than on matrix remodeling ones.

DISCUSSION

We have shown that TNFR1 expression on endothelial cells is required for valvular carditis in K/B.g7 mice. The absence of TNFR1 resulted in lower expression of VCAM1, fewer infiltrating cells, decreased lymphangiogenesis, and reduced expression of multiple inflammatory genes.

We explored many other inflammatory pathways that might contribute to valvular carditis in this model. We used a rigorous combination of *in vivo* antibody blockade of key cytokines plus whole animal and conditional knockout of critical genes involved in type 1, type 2, and type 3 cytokine responses. Through this extensive search, we discovered that these canonical pathways, exemplified by IFNγ, IL-4, and IL-17, are not required for valvular carditis in this model. Based on our findings here regarding TNFR1 and our prior work [14, 15], we therefore conclude that TNF and IL-6 produced by macrophages are the key cytokine drivers of valvular carditis.

TNFR1 is widely expressed, including as we have shown on most cell types in the cardiac valve (see Figure 3A), and TNF affects the biology of most cell types [16]. The finding that the absence of TNFR1 exclusively on endothelial cells was sufficient to protect against the development of valvular carditis was therefore somewhat surprising. We interpret this finding to indicate that TNF stimulation of endothelial cells via TNFR1 acts very early during the disease process, for instance by promoting upregulation of VCAM1 and the initial recruitment of inflammatory cells. This finding does not indicate, however, that the interaction of TNF with TNFR1 on other cell types, including immune cells and fibroblasts, is not important in the pathogenesis of valvular carditis. Indeed, the TNF:TNFR1 interaction may subsequently promote or sustain macrophage and/or fibroblast activation to drive chronic inflammation and fibrosis [49-51], and we are currently investigating these possibilities. However, without the disease-initiating activity of TNF:TNFR1 on endothelial cells, these downstream events are substantially impaired.

Our finding that endothelial cell expression of TNFR1 is critical for valvular carditis but not arthritis in the same mice is at first glance unexpected, given the well-recognized role of TNF in many forms of inflammatory arthritis in both humans and mice. The TNF independence of arthritis seems to be a peculiarity of the K/B.g7 mouse, however [15, 40-42]. We therefore suspect that models of inflammatory arthritis that do depend on TNF, endothelial cell TNFR1 expression could be important for arthritogenesis.

We have previously shown that blockade of IL-6 reduces the severity of valvular carditis and diminishes VCAM1 expression in the valve, similar to the effects of TNF blockade [15]. IL-6 is a well-known activator of the vascular endothelium [52], so we expect that TNF and IL-6 may both promote endothelial activation to drive valvular carditis in K/B.g7 mice, though apparently in a nonredundant fashion. It is possible that the cytokines act in series, with the TNF:TNFR1 interaction promoting additional endothelial cell production of IL-6 [52, 53]. The receptors and signaling modes utilized by IL-6 are complex, including trans-presentation of IL-6 by membrane-bound IL-6 receptor as well as trans-signaling mediated via a soluble IL-6 receptor [52], in addition to classical receptor:ligand signaling; all of these signaling modes depend on the gp130 receptor subunit shared by several other cytokine receptors. Thus, ablating IL-6 signaling in one specific cell type (as we have done here for TNFR1 in endothelial cells) is essentially impossible without affecting other cytokines that use the gp130 signaling molecule. Our finding that deletion of TNFR1 on endothelial cells significantly reduces mitral valve thickness but not entirely to that of non-arthritic control mice (Figure 4) is consistent with a model in which both IL-6 and TNF promote valvular carditis, with the action of TNF on endothelial cells serving a critical initiating role [15].

Although there are inherent limitations in extrapolating from specific mouse models to human disease states, our findings most directly inform our understanding of human autoimmune valvular carditis, for instance in the context of RHD. More broadly, many forms of inflammatory arthritis, including rheumatoid arthritis, lead to accelerated atherosclerosis and other forms of inflammatory cardiovascular disease [11, 54]. TNF appears to be a driver of this increased cardiac risk, by promoting endothelial dysfunction, and a meta-analysis has demonstrated that TNF inhibitor therapy can improve endothelial function in patients with rheumatoid arthritis [55]. Thus, understanding how the TNF:TNFR1 interaction promotes inflammatory cardiovascular pathology in the setting of systemic rheumatic diseases is directly relevant to improving long-term cardiac outcomes for patients.

Supplementary Material

Refer to Web version on PubMed Central for supplementary material.

Acknowledgments

We thank Dr. Rochus Voeller for contribution of human patient samples. We would like to thank the Center for Immunology Imaging Core, and the University of Minnesota Genomics Center for providing equipment, advice, and research support.

Funding

This study was funded by National Institutes of Health (R01-HL121093, T32-AI007313, T32-GM008244, R25-HL088728); Dr. Warren and Henrietta Warwick MD/PhD Fellowship; National Center for Advancing Translational

Sciences of the National Institutes of Health Award No. UL1TR000114; and University of Minnesota's NIH Clinical and Translational Science Award UL1TR002494. M.F. was supported by the Ministry of Science and Higher Education of the Russian Federation (Agreement No. 075-15-2022-301). M.F. and K.Z. were supported by Priority 2030 Federal Academic Leadership Program.

NONSTANDARD ABBREVIATIONS AND ACRONYMS

A	absorbance
AU	arbitrary units
EC	endothelial cell
GPI	glucose-6-phosphate isomerase
LA	left atrium
LV	left ventricle
ML	mural leaflet
MV	mitral valve
RHD	rheumatic heart disease
ROI	region of interest
SL	septal leaflet

REFERENCES

1. Frangogiannis NG. Inflammation in cardiac injury, repair and regeneration. Curr Opin Cardiol. 2015;30:240–5. [PubMed: 25807226]
2. Gawalko M, Balsam P, Lodzinski P, Grabowski M, Krzowski B, Opolski G and Kosiuk J. Cardiac Arrhythmias in Autoimmune Diseases. Circ J. 2020;84:685–694. [PubMed: 32101812]
3. Swirski FK and Nahrendorf M. Cardioimmunology: the immune system in cardiac homeostasis and disease. Nat Rev Immunol. 2018;18:733–744. [PubMed: 30228378]
4. Roy P, Orecchioni M and Ley K. How the immune system shapes atherosclerosis: roles of innate and adaptive immunity. Nat Rev Immunol. 2022;22:251–265. [PubMed: 34389841]
5. Meier LA and Binstadt BA. The Contribution of Autoantibodies to Inflammatory Cardiovascular Pathology. Front Immunol. 2018;9:911. [PubMed: 29755478]
6. Hojnik M, George J, Ziporen L and Shoenfeld Y. Heart valve involvement (Libman-Sacks endocarditis) in the antiphospholipid syndrome. Circulation. 1996;93:1579–87. [PubMed: 8608627]
7. Maksimowicz-McKinnon K and Mandell BF. Understanding valvular heart disease in patients with systemic autoimmune diseases. Cleve Clin J Med. 2004;71:881–5. [PubMed: 15570736]
8. Moyssakis I, Tektonidou MG, Vasilliou VA, Samarkos M, Votteas V and Moutsopoulos HM. Libman-Sacks endocarditis in systemic lupus erythematosus: prevalence, associations, and evolution. Am J Med. 2007;120:636–42. [PubMed: 17602939]
9. Passos LSA, Nunes MCP and Aikawa E. Rheumatic Heart Valve Disease Pathophysiology and Underlying Mechanisms. Front Cardiovasc Med. 2020;7:612716. [PubMed: 33537348]
10. Watkins DA, Johnson CO, Colquhoun SM, Karthikeyan G, Beaton A, Bukhman G, Forouzanfar MH, Longenecker CT, Mayosi BM, Mensah GA, Nascimento BR, Ribeiro ALP, Sable CA, Steer AC, Naghavi M, Mokdad AH, Murray CJL, Vos T, Carapetis JR and Roth GA. Global, Regional, and National Burden of Rheumatic Heart Disease, 1990-2015. N Engl J Med. 2017;377:713–722. [PubMed: 28834488]

11. Nurmohamed MT, Heslinga M and Kitas GD. Cardiovascular comorbidity in rheumatic diseases. Nat Rev Rheumatol. 2015;11:693–704. [PubMed: 26282082]
12. Monach PA, Mathis D and Benoist C. The K/BxN arthritis model. Curr Protoc Immunol. 2008;Chapter 15:Unit 15 22.
13. Binstadt BA, Hebert JL, Ortiz-Lopez A, Bronson R, Benoist C and Mathis D. The same systemic autoimmune disease provokes arthritis and endocarditis via distinct mechanisms. Proc Natl Acad Sci U S A. 2009;106:16758–63. [PubMed: 19805369]
14. Hobday PM, Auger JL, Schuneman GR, Haasken S, Verbeek JS and Binstadt BA. Fcgamma receptor III and Fcgamma receptor IV on macrophages drive autoimmune valvular carditis in mice. Arthritis Rheumatol. 2014;66:852–62. [PubMed: 24757138]
15. Meier LA, Auger JL, Engelson BJ, Cowan HM, Breed ER, Gonzalez-Torres MI, Boyer JD, Verma M, Marath A and Binstadt BA. CD301b/MGL2(+) Mononuclear Phagocytes Orchestrate Autoimmune Cardiac Valve Inflammation and Fibrosis. Circulation. 2018;137:2478–2493. [PubMed: 29386201]
16. Kalliolias GD and Ivashkiv LB. TNF biology, pathogenic mechanisms and emerging therapeutic strategies. Nat Rev Rheumatol. 2016;12:49–62. [PubMed: 26656660]
17. Pober JS. Endothelial activation: intracellular signaling pathways. Arthritis Res. 2002;4 Suppl 3:S109–16. [PubMed: 12110129]
18. Herbert DR, Holscher C, Mohrs M, Arendse B, Schwegmann A, Radwanska M, Leeto M, Kirsch R, Hall P, Mossmann H, Claussen B, Forster I and Brombacher F. Alternative macrophage activation is essential for survival during schistosomiasis and downmodulates T helper 1 responses and immunopathology. Immunity. 2004;20:623–35. [PubMed: 15142530]
19. Haas JD, Ravens S, Duber S, Sandrock I, Oberdorfer L, Kashani E, Chennupati V, Fohse L, Naumann R, Weiss S, Krueger A, Forster R and Prinz I. Development of interleukin-17-producing gammadelta T cells is restricted to a functional embryonic wave. Immunity. 2012;37:48–59. [PubMed: 22770884]
20. Van Hauwermeiren F, Armaka M, Karagianni N, Kranidioti K, Vandenbroucke RE, Loges S, Van Roy M, Staelens J, Puimege L, Palagani A, Berghe WV, Victoratos P, Carmeliet P, Libert C and Kollias G. Safe TNF-based antitumor therapy following p55TNFR reduction in intestinal epithelium. J Clin Invest. 2013;123:2590–603. [PubMed: 23676465]
21. Okabe K, Kobayashi S, Yamada T, Kurihara T, Tai-Nagara I, Miyamoto T, Mukouyama YS, Sato TN, Suda T, Ema M and Kubota Y. Neurons limit angiogenesis by titrating VEGF in retina. Cell. 2014;159:584–96. [PubMed: 25417109]
22. Lee DM, Friend DS, Gurish MF, Benoist C, Mathis D and Brenner MB. Mast cells: a cellular link between autoantibodies and inflammatory arthritis. Science. 2002;297:1689–92. [PubMed: 12215644]
23. Meier LA, Faragher JL, Osinski V, Auger JL, Voeller R, Marath A and Binstadt BA. CD47 Promotes Autoimmune Valvular Carditis by Impairing Macrophage Efferocytosis and Enhancing Cytokine Production. J Immunol. 2022;208:2643–2651. [PubMed: 35867674]
24. Zheng GX, Terry JM, Belgrader P, Ryvkin P, Bent ZW, Wilson R, Ziraldo SB, Wheeler TD, McDermott GP, Zhu J, Gregory MT, Shuga J, Montesclaros L, Underwood JG, Masquelier DA, Nishimura SY, Schnall-Levin M, Wyatt PW, Hindson CM, Bharadwaj R, Wong A, Ness KD, Beppu LW, Deeg HJ, McFarland C, Loeb KR, Valente WJ, Ericson NG, Stevens EA, Radich JP, Mikkelsen TS, Hindson BJ and Bielas JH. Massively parallel digital transcriptional profiling of single cells. Nat Commun. 2017;8:14049. [PubMed: 28091601]
25. Hao Y, Hao S, Andersen-Nissen E, Mauck WM 3rd, Zheng S, Butler A, Lee MJ, Wilk AJ, Darby C, Zager M, Hoffman P, Stoeckius M, Papalexi E, Mimitou EP, Jain J, Srivastava A, Stuart T, Fleming LM, Yeung B, Rogers AJ, McElrath JM, Blish CA, Gottardo R, Smibert P and Satija R. Integrated analysis of multimodal single-cell data. Cell. 2021;184:3573–3587 e29. [PubMed: 34062119]
26. Stuart T, Butler A, Hoffman P, Hafemeister C, Papalexi E, Mauck WM 3rd, Hao Y, Stoeckius M, Smibert P and Satija R. Comprehensive Integration of Single-Cell Data. Cell. 2019;177:1888–1902 e21. [PubMed: 31178118]

27. Butler A, Hoffman P, Smibert P, Papalexi E and Satija R. Integrating single-cell transcriptomic data across different conditions, technologies, and species. Nat Biotechnol. 2018;36:411–420. [PubMed: 29608179]
28. Satija R, Farrell JA, Gennert D, Schier AF and Regev A. Spatial reconstruction of single-cell gene expression data. Nat Biotechnol. 2015;33:495–502. [PubMed: 25867923]
29. Ritchie ME, Phipson B, Wu D, Hu Y, Law CW, Shi W and Smyth GK. limma powers differential expression analyses for RNA-sequencing and microarray studies. Nucleic Acids Res. 2015;43:e47. [PubMed: 25605792]
30. Chen EY, Tan CM, Kou Y, Duan Q, Wang Z, Meirelles GV, Clark NR and Ma'ayan A. Enrichr: interactive and collaborative HTML5 gene list enrichment analysis tool. BMC Bioinformatics. 2013;14:128. [PubMed: 23586463]
31. Kuleshov MV, Jones MR, Rouillard AD, Fernandez NF, Duan Q, Wang Z, Koplev S, Jenkins SL, Jagodnik KM, Lachmann A, McDermott MG, Monteiro CD, Gundersen GW and Ma'ayan A. Enrichr: a comprehensive gene set enrichment analysis web server 2016 update. Nucleic Acids Res. 2016;44:W90–7. [PubMed: 27141961]
32. Xie Z, Bailey A, Kuleshov MV, Clarke DJB, Evangelista JE, Jenkins SL, Lachmann A, Wojciechowicz ML, Kropiwnicki E, Jagodnik KM, Jeon M and Ma'ayan A. Gene Set Knowledge Discovery with Enrichr. Curr Protoc. 2021;1:e90. [PubMed: 33780170]
33. Monach P, Hattori K, Huang H, Hyatt E, Morse J, Nguyen L, Ortiz-Lopez A, Wu HJ, Mathis D and Benoist C. The K/BxN mouse model of inflammatory arthritis: theory and practice. Methods Mol Med. 2007;136:269–82. [PubMed: 17983155]
34. Nguyen LT, Jacobs J, Mathis D and Benoist C. Where FoxP3-dependent regulatory T cells impinge on the development of inflammatory arthritis. Arthritis Rheum. 2007;56:509–20. [PubMed: 17265486]
35. Matsumoto I, Maccioni M, Lee DM, Maurice M, Simmons B, Brenner M, Mathis D and Benoist C. How antibodies to a ubiquitous cytoplasmic enzyme may provoke joint-specific autoimmune disease. Nat Immunol. 2002;3:360–5. [PubMed: 11896391]
36. Krausgruber T, Blazek K, Smallie T, Alzabin S, Lockstone H, Sahgal N, Hussell T, Feldmann M and Udalova IA. IRF5 promotes inflammatory macrophage polarization and TH1-TH17 responses. Nat Immunol. 2011;12:231–8. [PubMed: 21240265]
37. Auger JL, Cowan HM, Engelson BJ, Kashem SW, Prinz I and Binstadt BA. Brief Report: Arthritis in KRN T Cell Receptor-Transgenic Mice Does Not Require Interleukin-17 or Th17 Cells. Arthritis Rheumatol. 2016;68:1849–55. [PubMed: 26882006]
38. Ohmura K, Nguyen LT, Locksley RM, Mathis D and Benoist C. Interleukin-4 can be a key positive regulator of inflammatory arthritis. Arthritis Rheum. 2005;52:1866–75. [PubMed: 15934072]
39. Van Dyken SJ and Locksley RM. Interleukin-4- and interleukin-13-mediated alternatively activated macrophages: roles in homeostasis and disease. Annu Rev Immunol. 2013;31:317–43. [PubMed: 23298208]
40. Kyburz D, Carson DA and Corr M. The role of CD40 ligand and tumor necrosis factor alpha signaling in the transgenic K/BxN mouse model of rheumatoid arthritis. Arthritis Rheum. 2000;43:2571–7. [PubMed: 11083282]
41. Ji H, Pettit A, Ohmura K, Ortiz-Lopez A, Duchatelle V, Degott C, Gravallese E, Mathis D and Benoist C. Critical roles for interleukin 1 and tumor necrosis factor alpha in antibody-induced arthritis. J Exp Med. 2002;196:77–85. [PubMed: 12093872]
42. Christianson CA, Corr M, Firestein GS, Mobargha A, Yaksh TL and Svensson CI. Characterization of the acute and persistent pain state present in K/BxN serum transfer arthritis. Pain. 2010;151:394–403. [PubMed: 20739123]
43. Ji H, Cao R, Yang Y, Zhang Y, Iwamoto H, Lim S, Nakamura M, Andersson P, Wang J, Sun Y, Dissing S, He X, Yang X and Cao Y. TNFR1 mediates TNF-alpha-induced tumour lymphangiogenesis and metastasis by modulating VEGF-C-VEGFR3 signalling. Nat Commun. 2014;5:4944. [PubMed: 25229256]
44. Baluk P, Yao LC, Feng J, Romano T, Jung SS, Schreiter JL, Yan L, Shealy DJ and McDonald DM. TNF-alpha drives remodeling of blood vessels and lymphatics in sustained airway inflammation in mice. J Clin Invest. 2009;119:2954–64. [PubMed: 19759514]

45. Sturzl M, Kunz M, Krug SM and Naschberger E. Angiocrine Regulation of Epithelial Barrier Integrity in Inflammatory Bowel Disease. Front Med (Lausanne). 2021;8:643607. [PubMed: 34409045]
46. Xu Y, Yuan L, Mak J, Pardanaud L, Caunt M, Kasman I, Larrivee B, Del Toro R, Suchting S, Medvinsky A, Silva J, Yang J, Thomas JL, Koch AW, Alitalo K, Eichmann A and Bagri A. Neuropilin-2 mediates VEGF-C-induced lymphatic sprouting together with VEGFR3. J Cell Biol. 2010;188:115–30. [PubMed: 20065093]
47. Garcia J, Sandi MJ, Cordelier P, Binetruy B, Pouyssegur J, Iovanna JL and Tournaire R. Tie1 deficiency induces endothelial-mesenchymal transition. EMBO Rep. 2012;13:431–9. [PubMed: 22421998]
48. Saharinen P, Eklund L and Alitalo K. Therapeutic targeting of the angiopoietin-TIE pathway. Nat Rev Drug Discov. 2017;16:635–661. [PubMed: 28529319]
49. Lin CC, Pan CS, Wang CY, Liu SW, Hsiao LD and Yang CM. Tumor necrosis factor-alpha induces VCAM-1-mediated inflammation via c-Src-dependent transactivation of EGF receptors in human cardiac fibroblasts. J Biomed Sci. 2015;22:53. [PubMed: 26173590]
50. Luo SF, Fang RY, Hsieh HL, Chi PL, Lin CC, Hsiao LD, Wu CC, Wang JS and Yang CM. Involvement of MAPKs and NF-kappaB in tumor necrosis factor alpha-induced vascular cell adhesion molecule 1 expression in human rheumatoid arthritis synovial fibroblasts. Arthritis Rheum. 2010;62:105–16. [PubMed: 20039412]
51. Wajant H and Siegmund D. TNFR1 and TNFR2 in the Control of the Life and Death Balance of Macrophages. Front Cell Dev Biol. 2019;7:91. [PubMed: 31192209]
52. Kang S and Kishimoto T. Interplay between interleukin-6 signaling and the vascular endothelium in cytokine storms. Exp Mol Med. 2021;53:1116–1123. [PubMed: 34253862]
53. Chi L, Li Y, Stehno-Bittel L, Gao J, Morrison DC, Stechschulte DJ and Dileepan KN. Interleukin-6 production by endothelial cells via stimulation of protease-activated receptors is amplified by endotoxin and tumor necrosis factor-alpha. J Interferon Cytokine Res. 2001;21:231–40. [PubMed: 11359654]
54. Semb AG, Ikdahl E, Wibetoe G, Crowson C and Rollefstad S. Atherosclerotic cardiovascular disease prevention in rheumatoid arthritis. Nat Rev Rheumatol. 2020;16:361–379. [PubMed: 32494054]
55. Ursini F, Leporini C, Bene F, D'Angelo S, Mauro D, Russo E, De Sarro G, Olivieri I, Pitzalis C, Lewis M and Grembiale RD. Anti-TNF-alpha agents and endothelial function in rheumatoid arthritis: a systematic review and meta-analysis. Sci Rep. 2017;7:5346. [PubMed: 28706194]

Highlights

- Endothelial cell-specific deletion of TNFR1 reduced the severity of autoimmune valvular carditis.
- Absence of TNFR1 on endothelial cells led to reduced expression of VCAM-1, macrophage infiltration, and pro-inflammatory gene expression.
- Typical type 1, 2, and 3 inflammatory pathways were not required for valvular carditis to develop.
- TNF and IL-6 are key drivers of autoimmune valvular carditis, and TNF acting on endothelial cells is a critical initiating event.

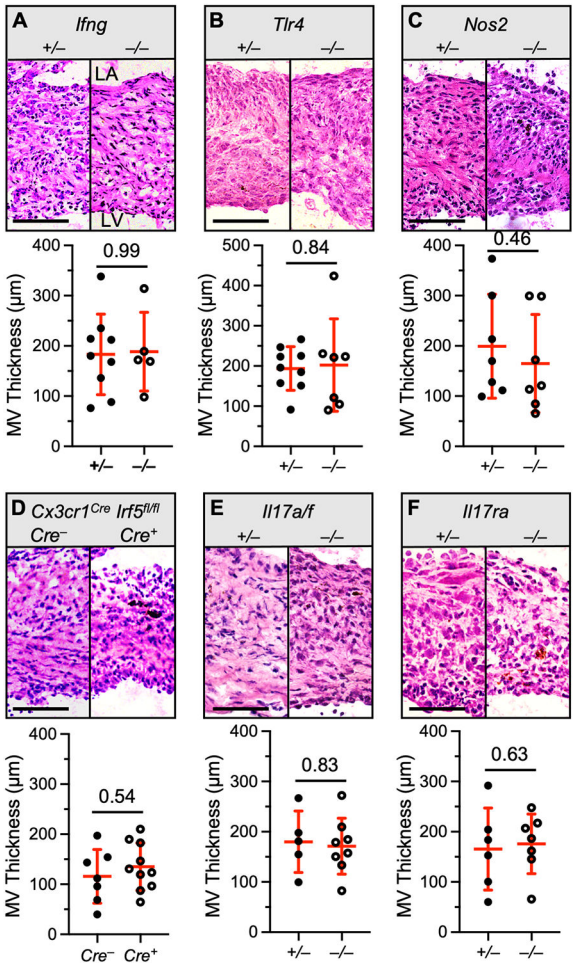

Figure 1. Canonical activators of type 1 and type 3 inflammation are not required for valvular carditis in K/B.g7 mice.

Top panels, H&E stained sections of representative mitral valve (MV) sections from K/B.g7 mice with indicated genotypes. **Bottom panels,** MV thickness measurements in the same mice. Orientation of left atrium (LA) and left ventricle (LV) across all panels is the same as denoted in **A**; all scale bars represent 50 μm. Data were analyzed using a two-tailed Mann-Whitney test. Data are represented as mean ± SD; p-values are displayed in each panel.

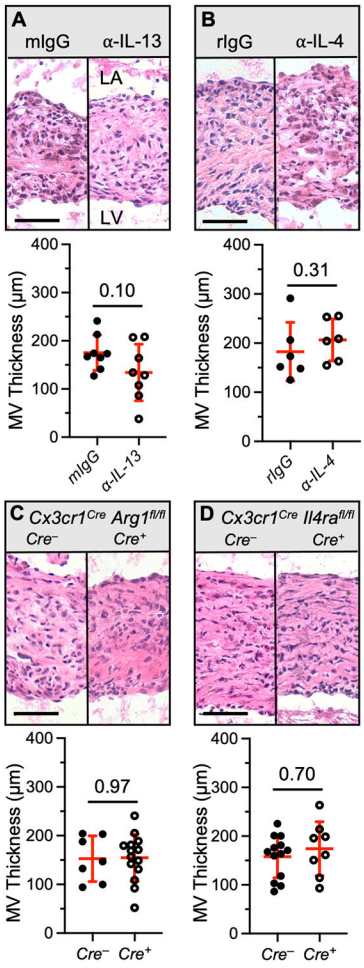

Figure 2. Type 2 inflammatory pathways are not required for valvular carditis in K/B.g7 mice.

Top panels, H&E staining of K/B.g7 MVs from mice that received indicated antibody blockade treatment and corresponding isotype control antibody mouse IgG (mIgG) or rat IgG (rIgG) or indicated *Cx3Cr1-Cre* mediated receptor deletion. **Bottom panels,** MV thickness measurements in the same mice. Orientation of left atrium (LA) and left ventricle (LV) across all panels is the same as denoted in **A**; all scale bars represent 50 μm. Data were analyzed using a two-tailed Mann-Whitney test. Data are represented as mean ± SD; p-values are displayed in each panel.

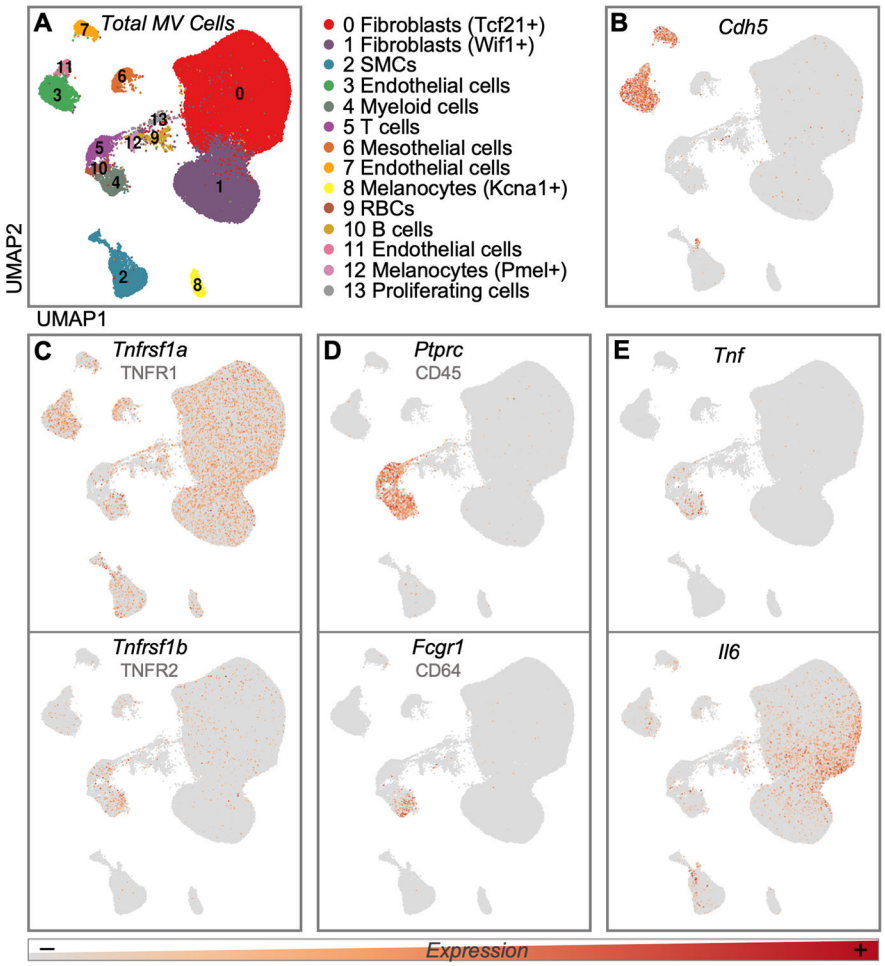

Figure 3. Single-cell RNA sequencing shows heterogenous expression of TNFR1 and confined expression of TNF.

A, Uniform Manifold Approximation and Projection (UMAP) visualization of scRNA sequenced K/B.g7 and B.g7 mitral valves (MVs). Cells were obtained from 3-, 8-, and 25-week-old mice (n=2 per age group from K/B.g7 and B.g7) MVs. Cell types characterizing each cluster are listed to the right of UMAP plot. Three endothelial cell clusters are distinguished by expression of *Vwf* (3), *Prox1* (7), *Hapln1* (11). Cluster 2 "SMCs" denote smooth muscle cells, cluster 9 "RBCs"; red blood cells. **B,** Transcript expression of *Cdh5* (VE Cadherin or CD144) overlayed on UMAP plot. **C,** *Tnfrsf1a* (encodes TNFR1, top) and *Tnfrsf1b* (encodes TNFR2, bottom). **D,** Expression of *Ptprc* (CD45, top) and *Fcgr1* (CD64, bottom). **E,** Expression of cytokines *Tnf* (TNF, top) and *Il6* (IL-6, bottom).

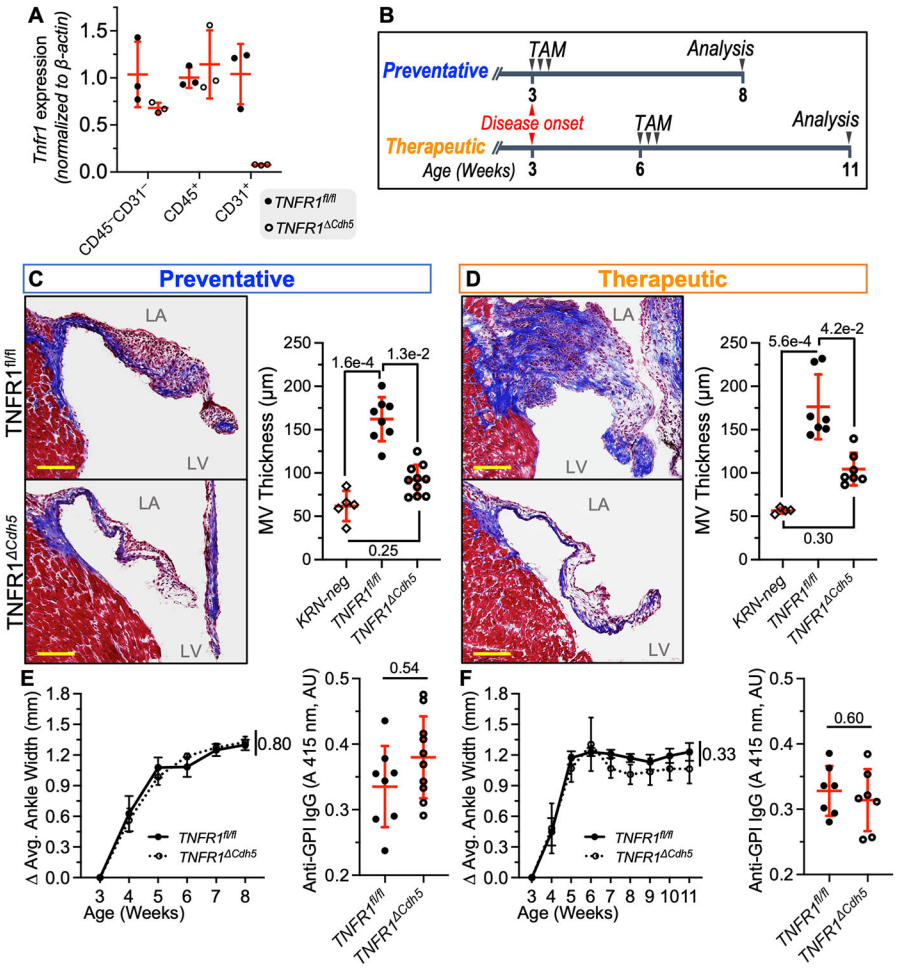

Figure 4. Endothelial deletion of TNFR1 prevents and reverses mitral valve disease.

A, qRT-PCR analysis of *Tnfr1* mRNA levels in TNFR1$^{fl/fl}$ (closed circle) and TNFR1$^{\Delta Cdh5}$ (open circle) mitral valve (MV) tissue from sorted CD45^{-}CD31^{-} cells, sorted hematopoietic (CD45^{+}) cells only, or sorted endothelial cells (CD31+) only. **B,** Schematic depiction of intraperitoneal (IP) tamoxifen (TAM) injections and end-point analysis for K/B.g7 TNFR1$^{fl/fl}$ and TNFR1$^{\Delta Cdh5}$ mice. Cre expression was induced by administration of tamoxifen (TAM) at 3 weeks (preventative) or 6 weeks of age (therapeutic). Hearts were analyzed 5 weeks after initiation of TAM. **C-D,** Trichrome stain of representative MV section from preventative **(C)** and therapeutic (**D**) Cre induction in TNFR1$^{fl/fl}$ (top image) and TNFR1$^{\Delta Cdh5}$ (bottom image) mice. Scale bars represent 100 μm. Left atrium (LA) and left ventricle (LV) are indicated, surrounding the mural leaflet. MV thickness measurements from non-inflamed (KRN-neg) and inflamed (TNFR1$^{fl/fl}$) littermate control mice are reported alongside TNFR1$^{\Delta Cdh5}$ mice (right). **E-F,** Average change in ankle thickness (left) and anti-GPI IgG titers (right) from preventative Cre (**E**) and therapeutic Cre (**F**). Anti-GPI IgG titers were read at an absorbance (A) of 415 nm and reported in arbitrary units (AU). MV thickness were analyzed with a non-parametric Kruskal-Wallis followed by Dunn's multiple comparisons. Anti-GPI titers were analyzed with a non-parametric two-tailed Mann-Whitney test. Change in ankle thickness was analyzed with a 2-way repeated

measures ANOVA with Sidak's multiple comparisons. Data are represented as mean ± SD; p-values are displayed in each panel.

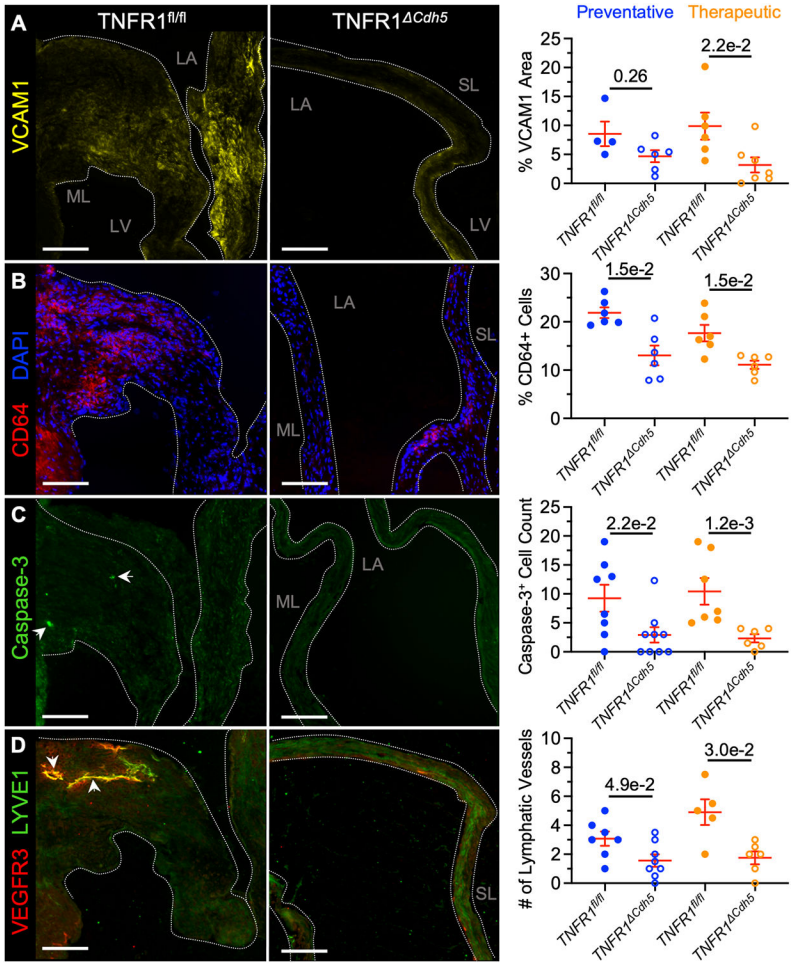

Figure 5. TNFR1$^{\Delta Cdh5}$ mice have reduced endothelial activation, immune cell infiltration, apoptotic cells, and lymphatic vessel development.

Representative immunofluorescent staining in MVs (white outline) from control TNFR1$^{fl/fl}$ (left image) and TNFR1$^{\Delta Cdh5}$ (right image) from therapeutic Cre induction. **A,** VCAM-1 (yellow) expression in mitral valve (MV). Area of positive VCAM1 signal as a percent of total MV area is quantified at right. Total images analyzed for preventative TNFR1$^{fl/fl}$, TNFR1$^{\Delta Cdh5}$ and therapeutic TNFR1$^{fl/fl}$, TNFR1$^{\Delta Cdh5}$ as follows: n=6, n=8, n=9, n=12. **B,** CD64 (red) and DAPI (blue) staining in MV. Total CD64 cells as a percent of total cell nuclei quantified. Total images analyzed as follows (n=12, n=11, n=11, n=11). **C,** VEGFR3 (red) and LYVE1 (green) staining. Colocalized signal (yellow) of both markers are lymphatic vessels (white arrows). Total number of lymphatic vessels is reported. Total images analyzed as follows (n=8, n=12, n=9, n=10). **D,** Cleaved caspase-3 (green) staining for apoptotic cells (white arrows). Total caspase-3+ cell count reported. Total images analyzed as follows (n=12, n=14, n=12, n=10). Data points may represent averaged image quantification from same specimen. Exposure set using a species-matched isotype control. Scale bars represent 100 μm. Left atrium (LA), left ventricle (LV), mural leaflet (ML), and septal leaflet (SL) are indicated. Orientation in **A** applies to all panels unless indicated otherwise. Data were analyzed using a two-tailed Mann-Whitney test. Data are represented as mean ± SD; p-values are displayed in each panel.

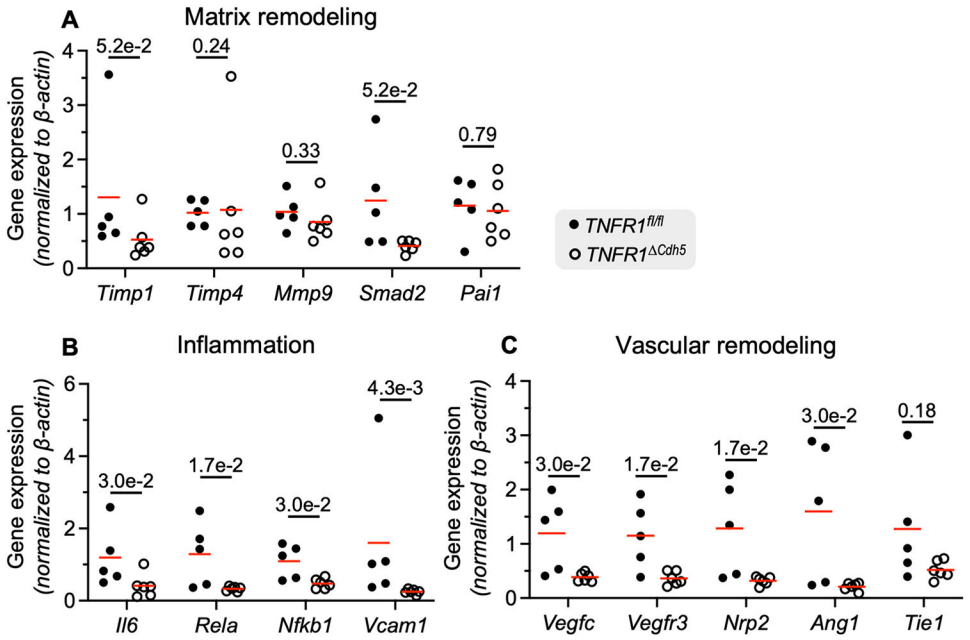

Figure 6. Deletion of endothelial TNFR1 reduces expression of genes associated with inflammatory and lymphangiogenic processes.

MVs from preventative Cre-induced TNFR1$^{\Delta Chd5}$ and control mice were analyzed via qRT-PCR for gene transcripts generally associated with **A,** Extracellular matrix remodeling; **B,** inflammation; **C,** angio- and lymphangiogenesis. Expression normalized to B-actin and 2^ΔΔCT values are displayed. Statistical analyses performed with unpaired, nonparametric Mann-Whitney test. Red bar indicates mean; p-values are displayed in each panel. Correction for multiple testing was not performed.